frontiers in Earth Science

ORIGINAL RESEARCH
published: 30 March 2022
doi: 10.3389/feart.2022.870332

Study on Pore Structure and the Microscopic Mechanism of the Difference in Petrophysical Properties of Tight Sandstone: A Case Study of the Chang 3 Member of Weibei Oilfield, Ordos Basin

Ying Tang[1,2], Jingchao Lei[3]*, Haoran Dong[1], Shihao Tan[1], Duanyue Ma[1], Nan Zhang[1] and Mingxian Wang[4]*

[1]College of Petroleum Engineering, Xi'an Shiyou University, Xi'an, China, [2]Beijing Key Laboratory of Unconventional Natural Gas Geological Evaluation and Development Engineering, Beijing, China, [3]Exploration Department of PetroChina Changqing Oilfield Company, Xi'an, China, [4]School of Earth Sciences and Engineering, Xi'an Shiyou University, Xi'an, China

OPEN ACCESS

Edited by:
Hu Li,
Southwest Petroleum University, China

Reviewed by:
Jun Wu,
China University of Geosciences, China
Wenjie Feng,
Yangtze University, China

***Correspondence:**
Jingchao Lei
364666192@qq.com
Ying Tang
tangying330@126.com

Specialty section:
This article was submitted to Economic Geology, a section of the journal Frontiers in Earth Science

Received: *09 February 2022*
Accepted: *07 March 2022*
Published: *30 March 2022*

Citation:
Tang Y, Lei J, Dong H, Tan S, Ma D, Zhang N and Wang M (2022) Study on Pore Structure and the Microscopic Mechanism of the Difference in Petrophysical Properties of Tight Sandstone: A Case Study of the Chang 3 Member of Weibei Oilfield, Ordos Basin. Front. Earth Sci. 10:870332. doi: 10.3389/feart.2022.870332

Tight sandstone reservoirs have complex pore throat structures and poor and large differences in petrophysical properties. In this study, taking the Chang 3 Member of Weibei Oilfield, Ordos Basin, China as an example, the microscopic mechanism of the differences in petrophysical properties of tight sandstone reservoirs was systematically studied by thin section observation, scanning electron microscope, whole-rock X-ray diffraction, and high-pressure mercury intrusion experiments. The research results show that the reservoir types of the Chang 3 Member are mainly feldspar lithic sandstone and lithic feldspar sandstone; the pore types include intergranular, intragranular dissolution pores, and a small amount of residual intergranular pores. Taking the permeability of 0.3×10^{-3} and 0.5×10^{-3} μm^2 as the boundary, we divided the samples involved in high-pressure mercury intrusion into three categories according to the permeability from high to low: Type I, Type II, and Type III. Their proportions were 31.4, 20.0, and 48.6%, respectively. The study found that the smaller the sorting coefficient, the poorer the petrophysical properties of the samples; the pore throat distribution of different samples gradually changed to a uniform double peak–dominated type. The permeability of tight sandstone reservoirs is contributed by a small part of pore throats with a large radius, while the reservoir space is mainly contributed by a large number of pores connected with small throats. The porosity is negatively and positively correlated with the median pressure and mercury injection tortuosity, respectively. In addition, the pore throat radius corresponding to the maximum permeability contribution rate, maximum pore throat radius, and sorting coefficient are all positively correlated with the permeability. In general, the areas with larger pore throat radius, lower pore throat tortuosity, and larger pore throat sorting coefficient can be regarded as favorable areas for Chang 3 tight sandstone reservoirs.

Keywords: Ordos Basin, tight sandstone, high-pressure mercury intrusion, difference in petrophysical properties, microscopic mechanism

1 INTRODUCTION

Conventional oil resources are decreasing day by day, and tight sandstone oil has become an important part of China's oil resources. Tight oil resources in major basins in China range from 8 to 10 billion tons. At present, China has built a highly industrialized tight oil–producing area in the Ordos Basin, and the producing layer is located in the Upper Triassic Yanchang Formation. Tight sandstone reservoirs are characterized by tight lithology, poor petrophysical properties, and strong microscopic heterogeneity (Yin et al., 2018; Yin and Ding, 2019; Dong et al., 2020; Hong et al., 2020; Santosh and Feng., 2020; Chen et al., 2021; Xue et al., 2021). Pore throats with different radii are obviously affected by complex capillary action and gravity, which lead to huge differences in seepage laws within different pore throat radii (Yin and Wu, 2020; Yoshida and Santosh., 2020; Zhang et al., 2020; Ding et al., 2021). Reservoir petrophysical properties are the final response of the microscopic pore throat structures (Yin et al., 2020a; Mohammed et al., 2021; Qie et al., 2021).

In recent years, the research methods of reservoir micro-heterogeneity have been continuously improved. For example, its development has gradually transitioned from conventional methods such as microscope observation and mercury intrusion to advanced methods such as nuclear magnetic resonance, high-pressure mercury intrusion, three-dimensional CT scanning, and laser focusing microscopy (Yin et al., 2020b; Hower and Groppo., 2021; Mirzaei-Paiaman and Ghanbarian., 2021; Wang and Wang., 2021). These methods directly or indirectly reflect the microscopic heterogeneity of the reservoir. The previous methods usually use the water displacement experiment to analyze the seepage characteristics of tight sandstone reservoirs, but there are few studies on the microscopic mechanism of the difference in petrophysical properties of tight sandstone reservoirs (Sun and Tang., 2006; Askarinezhad, 2010; Li et al., 2020; Mahmud et al., 2020; Lan et al., 2021). There is no doubt that the petrophysical properties of tight sandstone reservoirs are the key factors affecting oil content, oil saturation, production rate, and ultimate recovery factor of the reservoir (Barsotti et al., 2016; Fan et al., 2019; Yang et al., 2021). Therefore, an in-depth micro-mechanism study of the differences in petrophysical properties of tight sandstone reservoirs is necessary, which is of great significance to improve the accuracy of high-quality reservoir prediction (Zhang et al., 2019; Zuo et al., 2019).

In this study, taking the Chang 3 Member of Weibei Oilfield, Ordos Basin, China as an example, the microscopic mechanism of the difference in petrophysical properties of tight sandstone reservoirs was systematically studied by thin section observation, scanning electron microscope, whole-rock X-ray diffraction, and high-pressure mercury intrusion experiments. This study can provide a reliable basis for sweet spot prediction of tight sandstone reservoirs.

2 GEOLOGICAL BACKGROUND

The Ordos Basin in China has a total area of 370,000 km^2. The Upper Triassic Yanchang Formation has a monoclinic structure that is low in the northwest and high in the southeast. In addition, the slope of the Yanchang Formation is 8–20 m/km, and the formation dip is 1–2°. Affected by the tectonic activities of the Weibei Uplift Belt, some small-scale faults with small fault throws developed in this area (Nabawy et al., 2009; Li et al., 2016; Wang A. et al., 2018; Wang et al., 2020).

The study area, Weibei Oilfield, is located at the intersection part of the Weibei Uplift and Yishan Slope in the Ordos Basin, with an area of about 2028.9 km^2. The oil resources of the Yanchang Formation in the study area are 1.46×10^8t. According to the regionally developed stratigraphic correlation markers such as tuff, shale, and coal lines, the Upper Triassic Yanchang Formation is divided into Chang 10–Chang 1 Members from bottom to top (Gier et al., 2008; Gao et al., 2011; Dai et al., 2016; Cui et al., 2019). The Chang 10 to 7 Members (hereinafter referred to as C10–C7 in figures) were deposited in a lake transgression stage during which the lacustrine basin is formed and developed. During the deposition of the Chang 7 Member, the lacustrine basin was at its peak, and dark mudstone and interbedded oil shales of shallow and semi-deep lacustrine facies were developed. The deposition of Chang 6 to Chang 1 Members occurred during the delta construction in the lacustrine basin, followed by lake shrunk, and disappeared (Jia et al., 2012; Kwak et al., 2017). Among them, the Chang 3 Member (C3) is the main oil-bearing formation with an average burial depth of 550 m (**Figure 1**). The Chang 3 Member of Weibei Oilfield belongs to the front facies of braided river delta and develops underwater distributary channel, interdistributary bay, and mouth bar microfacies. Underwater distributary channel sand bodies are the main reservoirs (Li et al., 2019; Hong et al., 2020). The sand bodies are distributed in a north–south direction (**Figure 2**).

3 DATA AND METHODS

In this study, we completed thin section observation, scanning electron microscope test, particle size analysis, high-pressure mercury injection, whole-rock X-ray diffraction (XRD) analysis, and XRD clay mineral measurement of core samples from Chang 3 Member reservoirs in Weibei Oilfield.

A total of 234 cast thin sections were observed, and the mineral composition, pore type, particle sorting, and surface porosity parameters of the thin sections were determined using a Zeiss metallographic microscope (Axio Imager A2m) under the conditions of an indoor temperature of 25°C and a relative humidity of 50%. The detection basis is SY/T 5368-2000 "Rock Thin Section Identification". In addition, a total of 42 samples were observed by using an FEI QUANTA 250 environmental scanning electron microscope. The detection is based on GB/T 18295-2001 "Scanning Electron Microscope Analysis Method for Sandstone Samples of Oil and Gas Reservoirs".

The particle size distribution of 38 reservoir rock samples was tested by using an SFY-B2000 sonic vibration sieve particle size analyzer. Furthermore, reservoir rock grain size, percentage of different grain sizes, sorting coefficients, and kurtosis were obtained.

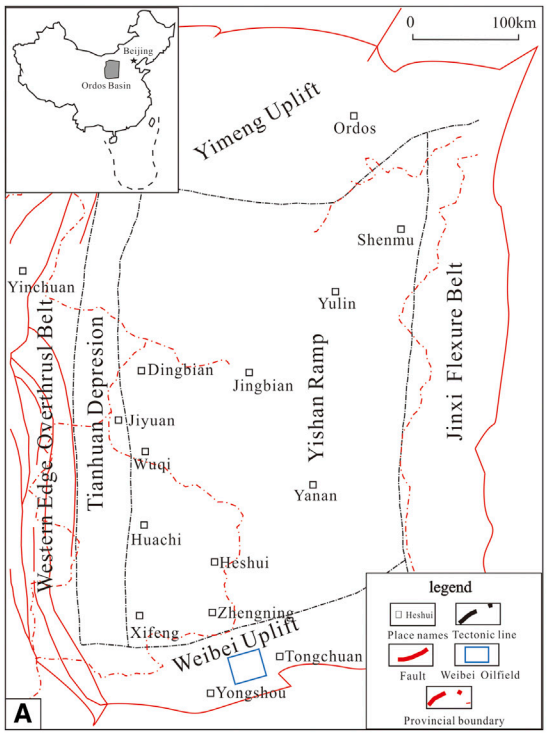

Erathem	System	Formation	Member	Thickness (m)	Evolution of the basin
Cenozonic	Quaternary			50-90	
Mesozoic	Lower Cretaceous			10-50	
	Jurassic	Zhiluo Formation		20-60	
		Yanan Formation		20-180	Lake basin filling Development stage of river and lake deltas
	Upper Triassic	Yan chang Formation	C2	0-165	Stable depression, lake basin shrinkage
			C3	100-165	
			C4+5	110-170	
			C6	100-150	
			C7	100-140	Strong depression
			C8	65-120	Lake basin expansion
			C9	90-110	The initial depression formed the lake basin
			C10	160-260	

B

FIGURE 1 | Location of the Weibei Oilfield **(A)** and stratigraphic column of the Yanchang Formation in the Ordos Basin **(B)** (modified from Wang et al., 2022).

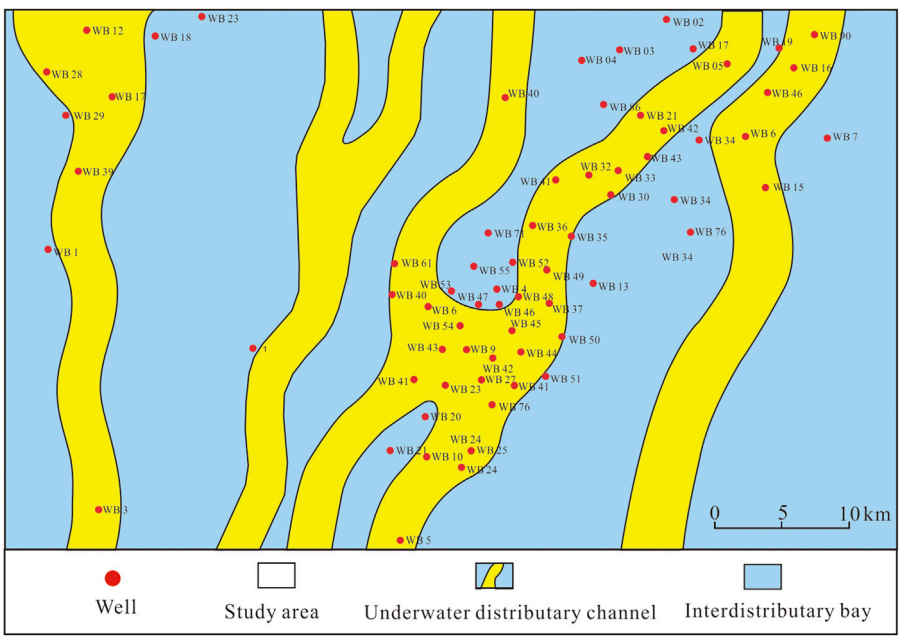

FIGURE 2 | Planar distribution of sedimentary facies in the Chang 3 Member of Weibei Oilfield.

An AutoPore IV 9505 automatic mercury porosimeter was used to complete the high-pressure mercury porosimetry of 35 tight sandstone sample gates at a temperature of 18°C and a relative humidity of 30%. The detection basis is SY/T 5346-2005 "Determination of Rock Capillary Pressure Curve". Furthermore, the porosity–permeability, mercury intrusion curves, and

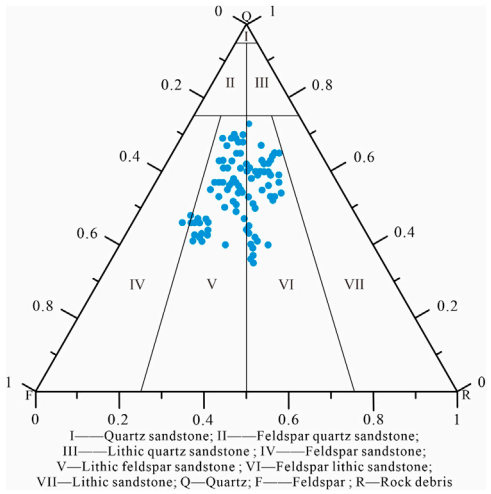

FIGURE 3 | Lithologic triangular diagram of sandstone in the Chang 3 Member in Weibei Oilfield.

characteristic parameters of pore throat structures of the samples were obtained.

Whole-rock X-ray diffraction (XRD) analysis and XRD clay mineral measurement were performed on 29 rock samples using a D/max-2600 X-ray diffractometer, and the contents of different types of minerals and clay minerals were obtained. The detection basis is SY/T 5163-2010 "X-ray Diffraction Analysis Method of Clay Minerals and Common Non-clay Minerals in Sedimentary Rocks".

4 RESULTS

4.1 Lithologies and Pore Types

The oil-bearing reservoirs in the Chang 3 Member are gray and gray–brown fine sandstones, with particle sizes mainly ranging from 0.06 to 0.25 mm. In addition, the clastic particles are mostly subangular to sub-round with moderate sorting and roundness. The lithologies of the reservoir are mainly feldspar lithic sandstone and lithic feldspar sandstone (**Figure 3**). Among the mineral components, the content of quartz is the largest (55.54%), followed by feldspar (24.09%) and debris (19.31%) (**Figures 4A,B**). According to the observation of microscopic thin sections, the composition of the Chang 3 Member comprises magmatic, metamorphic, and sedimentary rock debris. In the detrital composition, Q/F is 2.30 and Q/(F+R) is 1.29, indicating that the Chang 3 reservoir has high compositional maturity. In addition, the interstitials are dominated by carbonate cement and muddy matrix, with an average content of 8.28 and 3.80%, respectively; the content of clay minerals is low (average content of 3.8%) and dominated by kaolinite and illite (**Figures 4C,D**).

According to the observation results of the cast thin sections, the average face ratio of the Chang 3 Member is 7.61%, and its surface area is relatively low (the average value is 0.32 μm^{-1}). Statistics show that the shape factor of the target layer is relatively low (average 0.46), indicating that the pores are regular in shape. Moreover, the average coordination number of pore throats is 0.48 and the sorting coefficient is 9.78, indicating that the number of throats connected to pores is large and the pore heterogeneity is strong (**Table 1**). In addition, the proportions of three types of pores, namely, intergranular, intragranular dissolution pores, and residual intergranular pores, are 76.15, 18.15 and 5.7%, respectively. This shows that the pore types of the tight sandstone in the target layer are mainly intergranular and intragranular dissolution pores, and the proportion of residual intergranular pores is the lowest (**Figures 4C,D**).

4.2 Petrophysical Characteristics and Pore Structure Parameters

The petrophysical properties and pore structure parameters of the samples obtained based on the high-pressure mercury intrusion experiment are shown in **Table 2**. The porosity of the samples ranges from 2.20 to 14.97%, with an average value of 10.17%; the permeability ranges from 0.09×10^{-3} to 1.58×10^{-3} μm^2, with an average value of $0.44 \times 10^{-3} \mu m^2$. Referring to the classification criteria for ultra-low permeability reservoirs proposed by Yang and Fu (2012), we divided the samples into three categories with permeability (K) of 0.3×10^{-3} and 0.5×10^{-3} μm^2 as the boundaries: (Type I) $K \geq 0.5 \times 10^{-3}$ μm^2, (Type II) $0.5 \times 10^{-3} \mu m^2 > K \geq 0.3 \times 10^{-3}$ μm^2, and (Type III) $K < 0.3 \times 10^{-3}$ μm^2.

According to statistics, the proportions of Types I, II, and III samples in the Chang 3 Members are 31.4, 20.0, and 48.6%, respectively (**Figure 5**). From Type I to Type III reservoirs, with the decrease of the petrophysical properties of the samples, the average value of the maximum pore throat radius, median pore throat radius, and mercury withdrawal efficiency gradually decreased; and the average value of displacement pressure, median pressure, and residual mercury saturation gradually increased. Among them, the mercury withdrawal efficiency corresponds to the recovery factor in oilfield development, and the residual mercury saturation is the mercury saturation that remains in the rock sample when the injection pressure drops to a minimum value (Fan et al., 2020). It shows that the smaller the pore throat radius of the sample the greater the capillary resistance and the worse the petrophysical properties. Such reservoirs will show low recovery and high residual oil content in the actual development process.

From the correlation between permeability and porosity (**Figure 6**), it can be seen that there is a certain positive correlation between porosity and permeability, but the correlation is poor and the correlation coefficient R^2 is only 0.33. Some samples with less porosity can also obtain larger permeability, indicating that the porosity–permeability relationship of tight sandstone is significantly different from that of conventional sandstone. The research on the differences in petrophysical properties of this type of tight reservoirs should start from the perspective of microscopic pore throat structures (Nelson, 2009; Ryazanov, et al., 2014; Li et al., 2020).

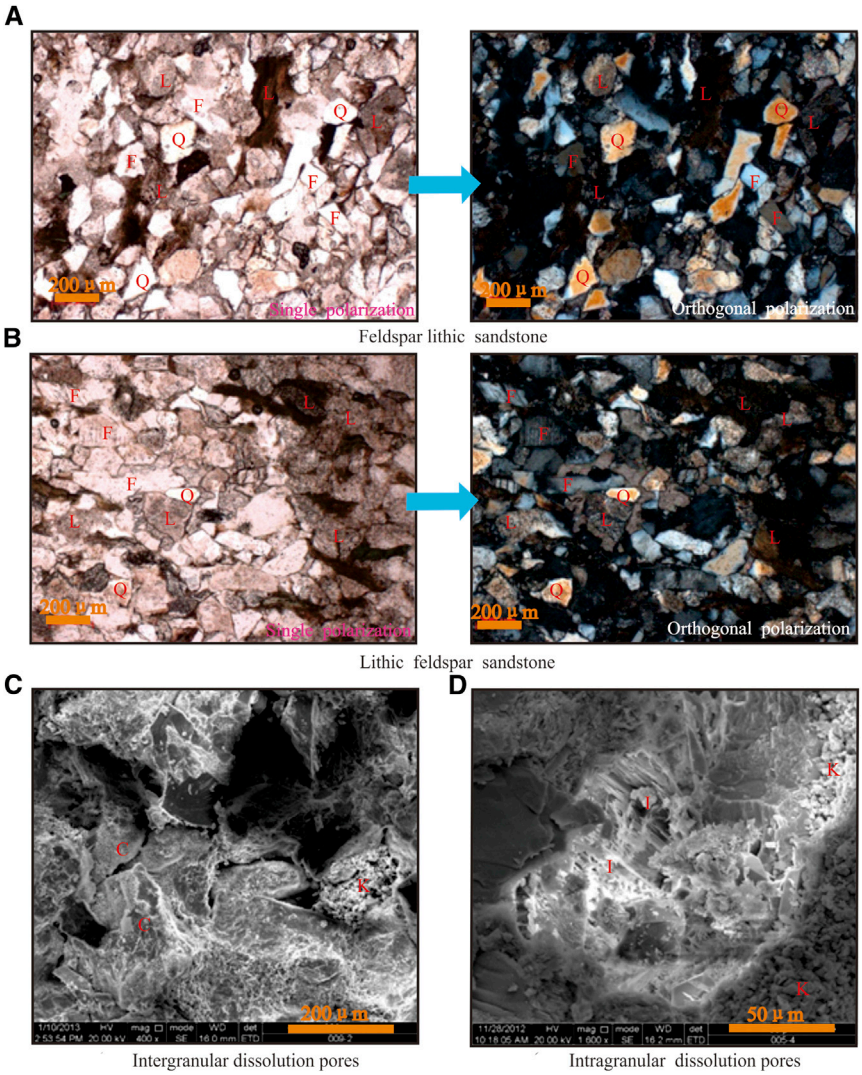

FIGURE 4 | Photomicrographs and scanning electron microscopy (SEM) images of the Chang 3 sandstone. Images on the left of **(A)** and **(B)** were test results under plane-polarized light, and images on the right of **(A)** and **(B)** were test results under cross-polarized light. **(A)** Well WB2, 544.60 m, ×50; **(B)** Well WB2, 547.71 m, ×50; **(C)** Well WB11, 395.84 m, intergranular pores with chlorite film on the surface of the particles. In addition, the pores are filled with book-like authigenic kaolinite; **(D)** Well WB15, 226.17 m; intragranular dissolution pores; and the pores are filled with kaolinite and illite. Q: quartz; R: rock debris; F: feldspar; C: chlorite; K: kaolinite; I: illite.

TABLE 1 | Types and characteristic parameters of pores analyzed for samples in the Chang 3 Member.

Horizon	Average face ratio	Average surface area (μm^{-1})	Average shape factor	Average coordination number	Sorting coefficient	Average pore throat ratio	Pore composition (%)		
							Residual intergranular pore	Intergranular dissolution pore	Intragranular dissolution pore
C3	7.61	0.32	0.46	0.48	9.78	9.50	5.70	76.15	18.15

5 DISCUSSION

5.1 Influence of Pore Throat Structures on Petrophysical Properties

The capillary pressure curve is the relationship between capillary pressure and mercury saturation, and a certain capillary pressure corresponds to a certain pore throat radius. From the perspective of pore structure, the capillary pressure curve can reflect the distribution of the pore and throats of the rock (Wang, 2008; Qiao et al., 2020). The shape of the capillary pressure curve is mainly controlled by the sorting of the pore throats and size of the throats. Sortability refers to the degree of dispersion of throat size

TABLE 2 | Petrophysical properties and pore structure parameters of the Chang 3 tight sandstone samples.

Type	Pore throat radius distribution	Well name	No	H(m)	ϕ (%)	k ($10^{-3}\mu m^2$)	Mercury intrusion parameters						
							P_d (MPa)	P_m (MPa)	S_{max} (%)	W_e (%)	S_r (%)	r_{max} (μm)	r_m (μm)
I	SP	WB11	WB11-15	397.45	13.14	1.58	0.35	4.47	82.20	41.36	48.20	2.17	0.17
I	SP	WB2	WB2-2	543.81	14.97	0.58	1.06	7.84	100.00	36.47	63.53	0.70	0.09
I	SP	WB2	WB2-39	550.88	13.79	1.16	0.64	4.57	100.00	37.15	63.80	1.15	0.16
I	DP	WB6	WB6-5	299.67	11.90	0.68	0.88	9.45	89.40	25.62	66.50	0.86	0.08
I	DP	WB9	WB9-19	509.18	2.20	0.63	1.11	41.06	60.00	18.67	48.80	0.67	0.02
I	DP	WB2	WB2-13	545.45	12.91	0.52	1.06	7.84	100.00	37.15	61.79	0.69	0.09
I	DP	WB7	WB7-2	409.23	14.56	0.91	0.35	4.37	90.80	37.15	69.40	2.12	0.17
I	DP	WB2	WB2-8	544.75	13.08	0.55	1.06	8.76	100.00	37.15	62.85	0.70	0.08
I	DP	WB2	WB2-23	547.15	14.27	0.94	0.62	6.41	100.00	37.15	61.06	1.18	0.12
I	DP	WB2	WB2-27	547.71	13.88	0.82	0.62	6.34	100.00	37.15	61.82	1.18	0.12
I	DP	WB2	WB2-47	553.68	11.89	0.94	0.48	4.70	100.00	37.15	65.13	1.53	0.16
Average					12.42	0.84	0.75	9.62	92.95	34.74	61.17	1.18	0.11
II	SP	WB11	WB11-4	394.91	8.93	0.38	0.75	8.45	88.20	33.33	58.80	1.00	0.09
II	SP	WB7	WB7-15	411.53	11.73	0.45	0.50	3.78	92.50	21.95	72.20	1.50	0.20
II	SP	WB2	WB2-43	551.75	5.78	0.33	5.04	26.22	100.00	37.15	52.18	0.15	0.03
II	SP	WB15	WB15-17	233.80	11.58	0.36	0.79	2.96	90.00	26.67	66.00	0.95	0.25
II	DP	WB6	WB6-52	306.43	10.66	0.49	0.70	7.63	92.80	18.97	75.20	1.07	0.10
II	DP	WB9	WB9-11	506.60	13.41	0.32	1.58	7.79	88.30	28.77	62.90	0.47	0.10
II	DP	WB2	WB2-17	546.12	3.89	0.34	6.42	31.93	100.00	37.15	56.73	0.12	0.02
II	DP	WB2	WB2-33	549.07	12.42	0.43	1.06	7.18	100.00	37.15	62.09	0.70	0.10
Average					9.80	0.39	2.10	11.99	93.98	30.14	63.26	0.74	0.11
III	SP	WB15	WB15-34	236.69	8.36	0.17	1.27	5.02	88.00	29.55	62.00	0.59	0.15
III	DP	WB15	WB15-4	225.99	7.90	0.12	2.01	10.44	86.00	32.56	58.00	0.37	0.07
III	DP	WB15	WB15-46	238.37	7.10	0.13	2.35	12.33	83.00	30.12	58.00	0.32	0.06
III	DP	WB15	WB15-55	246.74	8.71	0.17	1.30	6.02	89.00	21.35	70.00	0.58	0.12
III	DP	WB6	WB6-18	301.60	10.90	0.29	0.88	12.08	91.20	23.25	70.00	0.85	0.06
III	DP	WB6	WB6-31	303.69	12.56	0.25	1.30	10.71	93.50	23.74	71.30	0.58	0.07
III	DP	WB6	WB6-61	307.41	9.46	0.18	1.98	19.42	86.60	25.17	64.80	0.38	0.04
III	DP	WB6	WB6-44	305.46	8.42	0.22	1.70	9.45	91.20	19.08	73.80	0.44	0.08
III	DP	WB9	WB9-27	511.55	10.31	0.24	3.02	24.15	86.70	39.56	52.40	0.25	0.03
III	DP	WB9	WB9-5	504.62	10.21	0.23	2.78	11.24	89.50	33.85	59.20	0.27	0.07
III	DP	WB11	WB11-28	399.68	7.33	0.12	3.14	15.20	87.70	28.05	63.10	0.24	0.05
III	DP	WB11	WB11-37	401.41	7.51	0.13	2.92	15.11	85.20	26.29	62.80	0.26	0.05
III	DP	WB7	WB7-27	414.36	8.67	0.14	3.37	14.74	91.30	15.44	77.20	0.22	0.05
III	DP	WB7	WB7-35	416.88	10.07	0.14	3.31	16.47	92.80	17.46	76.60	0.23	0.05
III	DP	WB7	WB7-46	419.51	7.41	0.29	4.65	24.27	90.00	29.89	63.10	0.16	0.03
III	DP	WB13	WB13-2	309.25	6.30	0.09	4.81	19.99	90.00	24.22	68.20	0.16	0.04
Average					8.83	0.18	2.55	14.16	88.86	26.22	65.66	0.37	0.06

Notes: SP, single peak; DP, double peak; ϕ, porosity; k, permeability; P_d, displacement pressure; P_m, median pressure; S_{max}, maximum mercury saturation; W_e, mercury withdrawal efficiency; S_r, residual mercury saturation; r_{max}, maximum pore throat radius; r_m, median pore throat radius.

(Wang L. et al., 2018; Zhou et al., 2021). The more concentrated the distribution of throat size, the better the sorting, the longer the flat section in the middle of the capillary pressure curve, and the closer it is to parallel with the abscissa (Yang and Fu., 2012).

Moreover, the distribution interval and distribution shape of pore throat radius represent the proportion of the corresponding pore throat radius and strength of seepage capacity, respectively, and the pore structures represented by different peak shapes are also different (Yang et al., 2017). A single peak indicates that the pore type is relatively single, such as intergranular dissolution pores, intragranular dissolution pores, residual intergranular pores, or microcracks. The double peaks indicate that there are two main pore types combined, which together control the storage and permeability of the rock (Wang et al., 2017; Zhong, 2017; Wang R. et al., 2018). Due to the differences in the dominant pore type, the reservoir and percolation capacities of single peak–type or double peak–type reservoirs are also different.

The pore throat distribution of the Chang 3 Member reservoir is in the form of single peak and double peak, and double peak is dominant, with double peak samples accounting for 74% (**Figure 7**). A single peak–type pore throat distribution represents a single pore–type reservoir. The pore types of the single peak samples are mainly intergranular or intragranular dissolution, and the pore throat sorting is better and the average sorting coefficient is low (0.86). When the pore throat distribution is bimodal, it means that

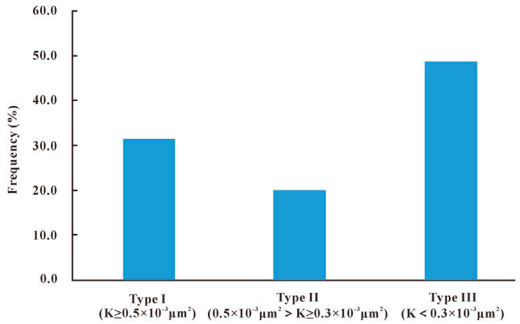

FIGURE 5 | Division of reservoir types in the Chang 3 Member.

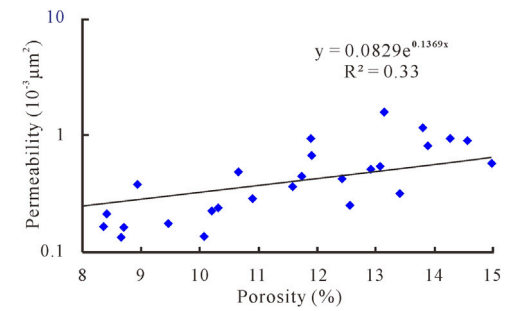

FIGURE 6 | Relationship between porosity and permeability of the tight sandstone samples in the Chang 3 Member.

the Chang 3 reservoir mainly develops pore throat spaces with two pore diameter ranges. This type of reservoir mainly develops intergranular and intragranular dissolution pores, which are poorly sorted and have a high average sorting coefficient (1.44). In addition, the average petrophysical properties of the double peak samples are worse than those of the single peak samples, indicating that tight reservoirs with a single pore type have better petrophysical properties.

Comparing the typical capillary pressure curves of the abovementioned three types of samples (**Figure 8**), it can be found that the capillary curves of the samples of Types I, II, and III are getting more and more smoother, indicating that the sorting of pore throats is gradually getting better. The sorting coefficients corresponding to these three types of reservoirs also decreased gradually from 0.3427 to 0.1018. That is, the smaller the pore throat sorting coefficient (the better the sorting), the worse the petrophysical properties of the samples. In addition, with the gradual improvement of the sorting properties of the samples, the pore throat radius distribution of the samples gradually changed to a single double peak shape. The double peak samples contain two pore types: intergranular and intragranular dissolution pores.

In addition, the lower limit of the pore throat radius of these three types of samples is about 0.0013 μm. However, only when the pore throat radius is greater than 0.004 μm, a certain amount of mercury exists in the pore throat. Mercury in Type I samples mainly exists in the pore throats controlled by the radius of 0.004–3.25 μm, and the permeability is the highest. Mercury in Type II samples mainly exists in the pore throats controlled by the radius of 0.004–1.3 μm, and the permeability is moderate. Mercury in Type III samples mainly exists in the pore throats controlled by the radius of 0.004–0.21 μm, and the permeability is the lowest. Samples with larger large pore throats have the best percolation performance.

Comparing the relationship among mercury injection amount, permeability contribution, and pore throat radius, it is found that as the pore throat radius decreases, the pore throat radius corresponding to the peak of permeability contribution is always larger than the pore throat radius corresponding to the

Horizon	Distribution of pore throat radius	Number of samples	Correlation diagram between mercury injection amount / permeability contribution rate and pore throat radius	Average porosity (%)	Average permeability (10^{-3}μm²)	Average sorting coefficient
Chang3	Single peak	8	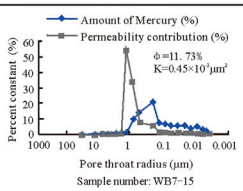	**11.04**	0.63	0.86
	Double peak	27	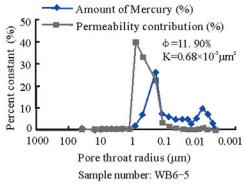	9.75	0.36	1.44

FIGURE 7 | Average of porosity, permeability, and sorting coefficient of single and double peak of the Chang 3 Member in the study area.

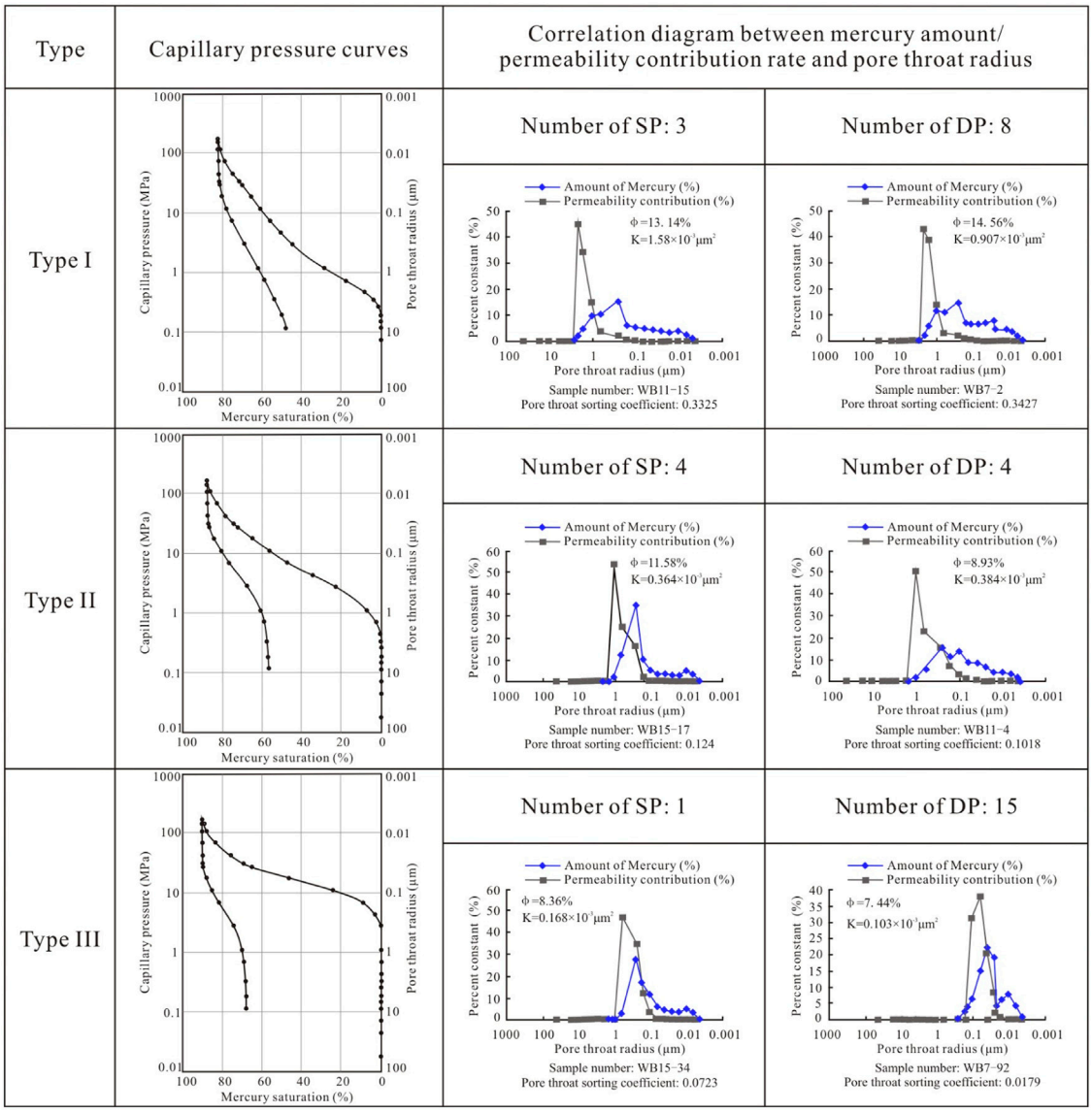

FIGURE 8 | Comparison of capillary pressure curves and mercury intrusion parameters of different types of samples in the Chang 3 Member. Notes: SP, single peak; DP, double peak.

peak mercury injection amount. Moreover, the pore throat radius covered by the peak mercury injection amount is larger. This shows that the reservoir permeability is contributed by a small part of pore throats with large radius, while the reservoir space is mainly contributed by a large number of pores connected with small throats.

5.2 Correlation Between Characteristic Parameters of Pore Structure and Petrophysical Properties

In this study, the high-pressure mercury intrusion experiments were used to obtain not only the petrophysical properties and pore throat structure parameters of the reservoir but also parameters such as structure coefficient and geometric factor (**Table 3**). Among them, the microscopic homogeneity coefficient represents the concentration degree of pore throats, and the pore structure coefficient represents the detour degree of fluid seepage in the pores. The larger the pore structure coefficient, the stronger the degree of bending and tortuousness of the pores (Zhong, 2017; Ren et al., 2019; Liu et al., 2020). Mercury injection and withdrawal tortuosity reflect the tortuosity of the pore throat morphology experienced by the nonwetting phase (mercury) when it enters and exits the cores, respectively (Song and Kovscek., 2016; Zhu et al., 2018; Shi et al., 2019). From the range of these characteristic parameters

TABLE 3 | Characteristic parameters of pore structures of the Chang 3 reservoirs.

Pore throat structure characteristic parameters	Chang 3 member		
	Minimum	Average	Maximum
Porosity (%)	2.20	10.18	14.97
Permeability ($10^{-3}\mu m^2$)	0.09	0.44	1.58
Pore throat radius corresponding to the maximum permeability contribution rate (μm)	0.10	0.45	1.60
Pore throat radius corresponding to the maximum mercury injection (μm)	0.04	0.18	0.25
Mercury injection tortuosity	0.30	1.20	2.93
Mercury withdrawal tortuosity	0.88	3.38	5.89
Relative sorting coefficient	0.77	1.01	1.41
Geometric factor	0.28	0.46	0.67
Maximum pore throat radius (μm)	0.12	0.71	2.17
Average pore throat radius (μm)	0.03	0.10	0.31
Median pore throat radius (μm)	0.02	0.09	0.25
Sorting coefficient	0.02	0.09	0.34
Displacement pressure (MPa)	0.35	1.88	6.42
Microscopic homogeneity coefficient	0.07	0.14	0.19
Pore structure coefficient	0.44	6.09	38.90

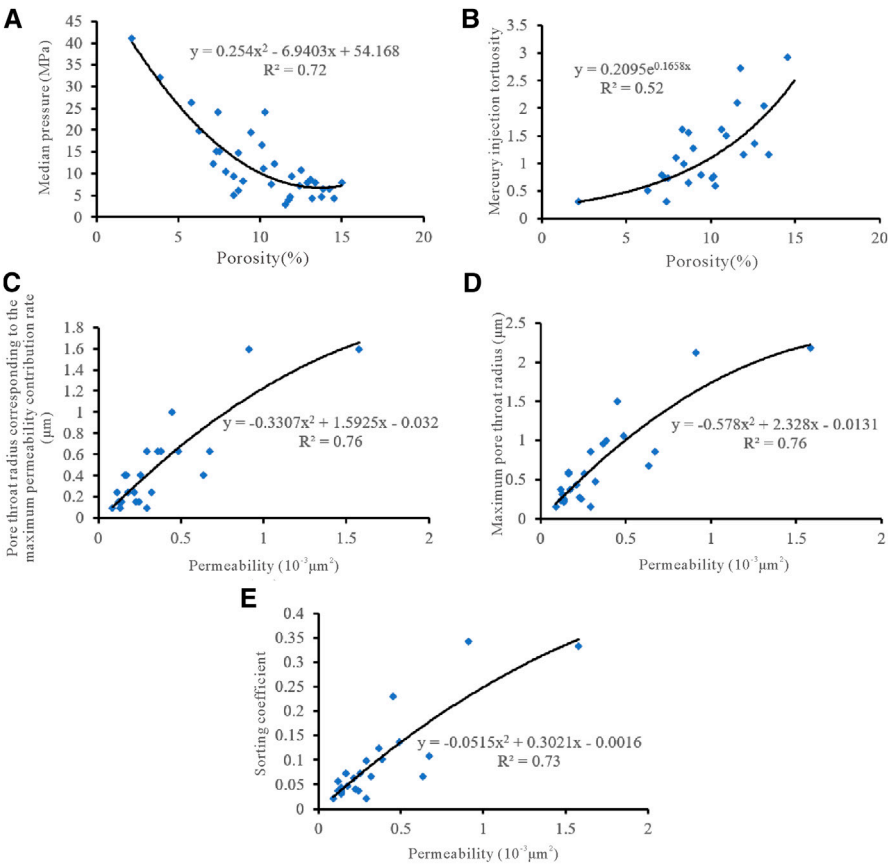

FIGURE 9 | Relationship between petrophysical properties and characteristic parameters of the pore structure of tight sandstone reservoirs in the Chang 3 Member.

and the relationship between the mercury injection amount/permeability contribution value and pore throat distribution (**Figures 7**, **8**), it can be found that due to the severe densification of the Chang 3 reservoir, the pore structure parameters are not much different, so the reservoir has good sorting. Because the pore throat radius tends to be small as a

whole, the number of effective throats in the reservoir is relatively small. The permeability of tight sandstone reservoirs is mainly contributed by a small fraction of larger pore throats. Ultimately, it is difficult for mercury to enter into the core and even more difficult to exit the core (the tortuosity of mercury withdrawal is greater than that of mercury injection).

From the correlation between the characteristic parameters of the pore structure of the Chang 3 Member and the petrophysical properties, it is found that the characteristic parameters of the pore structure that have a good correlation with the petrophysical properties include median pressure, mercury injection tortuosity, pore throat radius corresponding to the maximum permeability contribution rate, maximum pore throat radius, and sorting coefficient. Among them, the porosity is negatively and positively correlated with the median pressure and mercury injection tortuosity, respectively (**Figure 9**). This is because when the pore throat space is small, the capillary resistance is large, and the median pressure is also large. Mercury injection tortuosity reflects the degree of tortuosity of the pore throat morphology experienced by the nonwetting phase (mercury) when entering the core. When the tortuosity of mercury injection is large to a certain extent, the connectivity of pore throats will be impaired, but the increase of pore space will not be affected. The pore throat radius, maximum pore throat radius, and sorting coefficient corresponding to the maximum permeability contribution rate are positively correlated with the permeability (**Figure 9**). This is because the larger pore throat radius corresponding to the maximum permeability contribution rate and larger maximum pore throat radius are beneficial to the fluid flow in the pore throat space. The larger the sorting coefficient, the higher the probability of pore throats with larger radius and the higher the rock permeability.

6 CONCLUSION

1) In this study, taking the Chang 3 Member of Weibei Oilfield, Ordos Basin, China as an example, the microscopic mechanism of the difference in petrophysical properties of tight sandstone reservoirs was systematically studied by thin section observation, scanning electron microscope, whole-rock X-ray diffraction, and high-pressure mercury intrusion experiments.
2) The reservoir types of the Chang 3 Member are mainly feldspar lithic sandstone and lithic feldspar sandstone; the pore types include intergranular, intragranular dissolution pores, and a small amount of residual intergranular pores. Taking the permeability of 0.3×10^{-3} and 0.5×10^{-3} μm^2 as the boundary, we divided the samples involved in high-pressure mercury intrusion into three categories according to the permeability from high to low: Type I, Type II, and Type III. Their proportions were 31.4, 20.0, and 48.6%, respectively. Analysis of the three types of samples of high-pressure mercury injection data found that the smaller the sorting coefficient (sorting coefficient, the better, pore throat radius were similar to each other, the greater pore throat radius of low probability), sample properties, mercury injection dense sandstone core to overcome larger capillary force (expulsion pressure), and mercury withdrawal when residual mercury saturation is larger.
3) The study found that the smaller the sorting coefficient, the poorer the petrophysical properties of the samples and the pore throat distribution of different samples gradually changed to a uniform double peak–dominated type.
4) The permeability of tight sandstone reservoirs is contributed by a small part of pore throats with large radius, while the reservoir space is mainly contributed by a large number of pores connected with small throats. The porosity is negatively and positively correlated with the median pressure and mercury injection tortuosity, respectively. In addition, the pore throat radius corresponding to the maximum permeability contribution rate, maximum pore throat radius, and sorting coefficient are all positively correlated with the permeability. In general, the areas with larger pore throat radius, lower pore throat tortuosity, and larger pore throat sorting coefficient can be regarded as favorable areas for Chang 3 tight sandstone reservoirs.

DATA AVAILABILITY STATEMENT

The original contributions presented in the study are included in the article/Supplementary Material, further inquiries can be directed to the corresponding authors.

AUTHOR CONTRIBUTIONS

YT and JL contributed to the method and writing of the manuscript. HD, ST, DM, NZ, and MW contributed to experiments.

FUNDING

This research was supported by the PetroChina Innovation Foundation (No. 2020D-5007-0202), the Opening Foundation of Provincial and Ministerial Key Laboratory of China University of Geosciences (Beijing) (No. 20210102), the Natural Science Basic Research Plan in Shaanxi Province of China (No. 2021JQ-598), and the National Natural Science Foundation of China (No. 52104031).

REFERENCES

Askarinezhad, R. (2010). A New Statistical Approach to Pore/throat Size Distribution of Porous media Using Capillary Pressure Distribution Concept. *J. Pet. Sci. Eng.* 75 (1-2), 100–104. doi:10.1016/j.petrol.2010.10.011

Barsotti, E., Tan, S. P., Saraji, S., Piri, M., and Chen, J.-H. (2016). A Review on Capillary Condensation in Nanoporous media: Implications for Hydrocarbon Recovery from Tight Reservoirs. *Fuel* 184, 344–361. doi:10.1016/j.fuel.2016.06.123

Bukar, M., Worden, R. H., Bukar, S., and Shell, P. (2021). Diagenesis and its Controls on Reservoir Quality of the Tambar Oil Field, Norwegian North Sea. *Energ. Geosci.* 2 (1), 10–31. doi:10.1016/j.engeos.2020.07.002

Chen, G. B., Li, T., Yang, L., Zhang, G. H., Li, J. W., and Dong, H. J. (2021). Mechanical Properties and Failure Mechanism of Combined Bodies with Different Coal-Rock Ratios and Combinations. *J. Mining Strata Control. Eng.* 3 (2), 023522. doi:10.13532/j.jmsce.cn10-1638/td.20210108.001

Cui, J., Zhu, R., Mao, Z., and Li, S. (2019). Accumulation of Unconventional Petroleum Resources and Their Coexistence Characteristics in Chang7 Shale Formations of Ordos Basin in central China. *Front. Earth Sci.* 13 (3), 575–587. doi:10.1007/s11707-019-0756-x

Dai, Q., Luo, Q., Chen, Z., Lu, C., Zhang, Y., Lu, S., et al. (2016). Pore Structure Characteristics of Tight-Oil sandstone Reservoir Based on a New Parameter Measured by NMR experiment: A Case Study of Seventh Member in Yanchang Formation, Ordos Basin. *Acta Petrolei Sinica* 37 (7), 887–897. doi:10.7623/syxb201607007

Ding, F., Xie, C., Zhou, X., Jiang, C., Li, K., Wan, L., et al. (2021). Defining Stratigraphic Oil and Gas Plays by Modifying Structural Plays: A Case Study from the Xihu Sag, east China Sea Shelf Basin. *Energ. Geosci.* 2 (1), 41–51. doi:10.1016/j.engeos.2020.08.002

Dong, S., Zeng, L., Lyu, W., Xia, D., Liu, G., Wu, Y., et al. (2020). Fracture Identification and Evaluation Using Conventional Logs in Tight Sandstones: A Case Study in the Ordos Basin, China. *Energ. Geosci.* 1 (3–4), 115–123. doi:10.1016/j.engeos.2020.06.003

Fan, C., Li, H., Qin, Q., Shang, L., Yuan, Y., and Li, Z. (2020). Formation Mechanisms and Distribution of Weathered Volcanic Reservoirs: A Case Study of the Carboniferous Volcanic Rocks in Northwest Junggar Basin, China. *Energy Sci. Eng.* 8 (8), 2841–2858. doi:10.1002/ese3.702

Fan, C., Zhong, C., Zhang, Y., Qin, Q., and He, S. (2019). Geological Factors Controlling the Accumulation and High Yield of Marine-Facies Shale Gas: Case Study of the Wufeng-Longmaxi Formation in the Dingshan Area of Southeast Sichuan, China. *Acta Geologica Sinica - English Edition* 93 (3), 536–560. doi:10.1111/1755-6724.13857

Gao, H., Xie, W., Yang, J., Zhang, C., and Sun, W. (2011). Pore Throat Characteristics of Extra -ultra Low Permeability sandstone Reservoir Based on Constant-Rate Mercury Penetration Technique. *Pet. Geology. Exp.* 33, 206–214. doi:10.1007/s12182-011-0123-3

Gier, S., Worden, R. H., Johns, W. D., and Kurzweil, H. (2008). Diagenesis and Reservoir Quality of Miocene Sandstones in the Vienna Basin, Austria. *Mar. Pet. Geology.* 25 (8), 681–695. doi:10.1016/j.marpetgeo.2008.06.001

Hong, D., Cao, J., Wu, T., Dang, S., Hu, W., and Yao, S. (2020). Authigenic clay Minerals and Calcite Dissolution Influence Reservoir Quality in Tight Sandstones: Insights from the central Junggar Basin, NW China. *Energ. Geosci.* 1 (1–2), 8–19. doi:10.1016/j.engeos.2020.03.001

Hower, J. C., and Groppo, J. G. (2021). Rare Earth-Bearing Particles in Fly Ash Carbons: Examples from the Combustion of Eastern Kentucky Coals. *Energ. Geosci.* 2 (2), 90–98. doi:10.1016/j.engeos.2020.09.003

Jia, C., Zou, C., Li, J., Li, D., and Zheng, M. (2012). Assessment Criteria, Main Types, Basic Features and Resource Prospects of the Tight Oil in China. *Acta Petrolei Sinica* 33 (3), 343–350. doi:10.1016/0031-9384(73)90235-7

Kwak, D., Han, S., Han, J., Wang, J., Lee, J., and Lee, Y. (2018). An Experimental Study on the Pore Characteristics Alteration of Carbonate during Waterflooding. *J. Pet. Sci. Eng.* 161, 349–358. doi:10.1016/j.petrol.2017.11.051

Lan, S. R., Song, D. Z., Li, Z. L., and Liu, Y. (2021). Experimental Study on Acoustic Emission Characteristics of Fault Slip Process Based on Damage Factor. *J. Mining Strata Control. Eng.* 3 (3), 023038. doi:10.13532/j.jmsce.cn10-1638/td.20210510.002

Li, G., Qin, Y., Shen, J., Wu, M., Li, C., Wei, K., et al. (2019). Geochemical Characteristics of Tight sandstone Gas and Hydrocarbon Charging History of Linxing Area in Ordos Basin, China. *J. Pet. Sci. Eng.* 177, 198–207. doi:10.1016/j.petrol.2019.02.023

Li, H., Li, Y., Chen, S., Guo, J., Wang, K., and Luo, H. (2016). Effects of Chemical Additives on Dynamic Capillary Pressure during Waterflooding in Low Permeability Reservoirs. *Energy Fuels* 30 (9), 7082–7093. doi:10.1021/acs.energyfuels.6b01272

Li, Y., Zhou, D., Wang, W., Jiang, T., and Xue, Z. (2020). Development of Unconventional Gas and Technologies Adopted in China. *Energ. Geosci.* 1 (1–2), 55–68. doi:10.1016/j.engeos.2020.04.004

Liu, Y., Gao, M., and Zhao, H. (2020). Detection of Overlying Rock Structure and Identification of Key Stratum by Drilling and Logging Technology. *J. Mining Strata Control. Eng.* 2 (2), 81–89. doi:10.13532/j.jmsce.cn10-1638/td.2020.02.004

Mahmud, H. B., Bin Muhammad Hisham, M. H., Mahmud, W. M., Leong, V. H., and Shafiq, M. U. (2020). Petrophysical Interpretations of Subsurface Stratigraphic Correlations, Baram Delta, Sarawak, Malaysia. *Energ. Geosci.* 1 (3–4), 100–114. doi:10.1016/j.engeos.2020.04.005

Mirzaei-Paiaman, A., and Ghanbarian, B. (2021). A New Methodology for Grouping and Averaging Capillary Pressure Curves for Reservoir Models. *Energ. Geosci.* 2 (1), 52–62. doi:10.1016/j.engeos.2020.09.001

Nabawy, B. S., Géraud, Y., Rochette, P., and Bur, N. (2009). Pore-throat Characterization in Highly Porous and Permeable Sandstones. *Bulletin* 93 (6), 719–739. doi:10.1306/03160908131

Nelson, P. H. (2009). Pore-throat Sizes in Sandstones, Tight Sandstones, and Shales. *Bulletin* 93 (3), 329–340. doi:10.1306/10240808059

Qiao, J., Zeng, J., Jiang, S., and Wang, Y. (2020). Impacts of Sedimentology and Diagenesis on Pore Structure and Reservoir Quality in Tight Oil sandstone Reservoirs: Implications for Macroscopic and Microscopic Heterogeneities. *Mar. Pet. Geology.* 111, 279–300. doi:10.1016/j.marpetgeo.2019.08.008

Qie, L., Shi, Y. N., and Liu, J. S. (2021). Experimental Study on Grouting Diffusion of Gangue Solid Filling Bulk Materials. *J. Mining Strata Control. Eng.* 3 (2), 023011. doi:10.13532/j.jmsce.cn10-1638/td.20201111.001

Ren, D., Zhou, D., Liu, D., Dong, F., Ma, S., and Huang, H. (2019). Formation Mechanism of the Upper Triassic Yanchang Formation Tight sandstone Reservoir in Ordos Basin-Take Chang 6 Reservoir in Jiyuan Oil Field as an Example. *J. Pet. Sci. Eng.* 178, 497–505. doi:10.1016/j.petrol.2019.03.021

Ryazanov, A. V., Sorbie, K. S., and van Dijke, M. I. J. (2014). Structure of Residual Oil as a Function of Wettability Using Pore-Network Modelling. *Adv. Water Resour.* 63, 11–21. doi:10.1016/j.advwatres.2013.09.012

Santosh, M., and Feng, Z. Q. (2020). New Horizons in Energy Geoscience. *Energ. Geosci.* 1 (1–2), A1. doi:10.1016/j.engeos.2020.05.005

Shi, B., Chang, X., Yin, W., Li, Y., and Mao, L. (2019). Quantitative Evaluation Model for Tight sandstone Reservoirs Based on Statistical Methods - A Case Study of the Triassic Chang 8 Tight Sandstones, Zhenjing Area, Ordos Basin, China. *J. Pet. Sci. Eng.* 173, 601–616. doi:10.1016/j.petrol.2018.10.035

Song, W., and Kovscek, A. R. (2016). Direct Visualization of Pore-Scale Fines Migration and Formation Damage during Low-Salinity Waterflooding. *J. Nat. Gas Sci. Eng.* 34, 1276–1283. doi:10.1016/j.jngse.2016.07.055

Sun, W., and Tang, G. Q. (2006). Visual Study of Water Injection in Low Permeable sandstone. *J. Can. Pet. Techn.* 45 (11), 21–26. doi:10.2118/06-11-02

Wang, A., Zhong, D., Zhu, H., Guo, L., Li, Z., Jiang, Y., et al. (2018a). Depositional and Diagenetic Controls on the Reservoir Quality of Upper Triassic Chang-7 Tight Oil Sandstones, Southwestern Ordos basin, China. *Geosci. J.* 23 (3), 471–488. doi:10.1007/s12303-018-0042-z

Wang, E., Liu, G., Pang, X., Wu, Z., Li, C., Bai, H., et al. (2020). Sedimentology, Diagenetic Evolution, and Sweet Spot Prediction of Tight sandstone Reservoirs: A Case Study of the Third Member of the Upper Paleogene Shahejie Formation, Nanpu Sag, Bohai Bay Basin, China. *J. Pet. Sci. Eng.* 186, 106718. doi:10.1016/j.petrol.2019.106718

Wang, J., and Wang, X. L. (2021). Seepage Characteristic and Fracture Development of Protected Seam Caused by Mining Protecting Strata. *J. Mining Strata Control. Eng.* 3 (3), 033511. doi:10.13532/j.jmsce.cn10-1638/td.20201215.001

Wang, L., Zhao, N., Sima, L., Meng, F., and Guo, Y. (2018b). Pore Structure Characterization of the Tight Reservoir: Systematic Integration of Mercury

Injection and Nuclear Magnetic Resonance. *Energy Fuels* 32 (7), 7471–7484. doi:10.1021/acs.energyfuels.8b01369

Wang, R., Chi, Y., Zhang, L., He, R., Tang, Z., and Liu, Z. (2018c). Comparative Studies of Microscopic Pore Throat Characteristics of Unconventional Superlow Permeability sandstone Reservoirs: Examples of Chang 6 and Chang 8 Reservoirs of Yanchang Formation in Ordos Basin, China. *J. Pet. Sci. Eng.* 160, 72–90. doi:10.1016/j.petrol.2017.10.030

Wang, R. (2008). *Microscopic Characteristics of Ultra-low Permeability sandstone Reservoir*. Beijing: Petroleum Industry Press.

Wang, R., Xu, G., Wu, X., Liu, Z., and Chi, Y. (2017). Comparative Studies of Three Nonfractured Unconventional Sandstone Reservoirs with Superlow Permeability: Examples of the Upper Triassic Yanchang Formation in the Ordos Basin, China. *Energy Fuels* 31 (1), 107–118. doi:10.1021/acs.energyfuels.6b01616

Wang, S. L., Li, H., Lin, L. F., and Yin, S. (2022). Development Characteristics and Finite Element Simulation of Fractures in Tight Oil Sandstone Reservoirs of Yanchang Formation in Western Ordos Basin. *Front. Earth Sci.* 9, 1–10. doi:10.3389/feart.2021.823855

Xue, F., Liu, X. X., and Wang, T. Z. (2021). Research on Anchoring Effect of Jointed Rock Mass Based on 3D Printing and Digital Speckle Technology. *J. Mining Strata Control. Eng.* 3 (2), 023013. doi:10.13532/j.jmsce.cn10-1638/td.20201020.001

Yang, H., and Fu, J. (2012). *Exploration Theory and Technology for Ultra-low Permeability Reservoirs*. Beijing: Petroleum Industry Press.

Yang, H., Liang, X., Niu, X., Feng, S., and You, Y. (2017). Geological Conditions for continental Tight Oil Formation and the Main Controlling Factors for the Enrichment: A Case of Chang7 Member, Triassic Yanchang Formation, Ordos Basin, NW China. *Pet. Exploration Dev.* 44 (1), 12–20. doi:10.1016/S1876-3804(17)30003-4

Yang, J. X., Luo, M. K., Zhang, X. W., Huang, N., and Hou, S. J. (2021). Mechanical Properties and Fatigue Damage Evolution of Granite under Cyclic Loading and Unloading Conditions. *J. Mining Strata Control. Eng.* 3 (3), 033016. doi:10.13532/j.jmsce.cn10-1638/td.20210510.001

Yin, S., and Ding, W. (2019). Evaluation Indexes of Coalbed Methane Accumulation in the strong Deformed Strike-Slip Fault Zone Considering Tectonics and Fractures: A 3D Geomechanical Simulation Study. *Geol. Mag.* 156 (6), 1052–1068. doi:10.1017/s0016756818000456

Yin, S., Dong, L., Yang, X., and Wang, R. (2020b). Experimental Investigation of the Petrophysical Properties, Minerals, Elements and Pore Structures in Tight Sandstones. *J. Nat. Gas Sci. Eng.* 76 (1), 103189–103214. doi:10.1016/j.jngse.2020.103189

Yin, S., Lv, D., and Ding, W. (2018). New Method for Assessing Microfracture Stress Sensitivity in Tight sandstone Reservoirs Based on Acoustic Experiments. *Int. J. Geomechanics* 18 (4), 1–11. doi:10.1061/(ASCE)GM.1943-5622.0001100

Yin, S., Tian, T., Wu, Z., and Li, Q. (2020a). Developmental Characteristics and Distribution Law of Fractures in a Tight sandstone Reservoir in a Low-amplitude Tectonic Zone, Eastern Ordos Basin, China. *Geol. J.* 55 (2), 1546–1562. doi:10.1002/gj.3521

Yin, S., and Wu, Z. (2020). Geomechanical Simulation of Low-Order Fracture of Tight sandstone. *Mar. Pet. Geology.* 117, 104359–104410. doi:10.1016/j.marpetgeo.2020.104359

Yoshida, M., and Santosh, M. (2020). Energetics of the Solid Earth: An Integrated Perspective. *Energ. Geosci.* 1 (1–2), 28–35. doi:10.1016/j.engeos.2020.04.001

Zhang, B., Shen, B., and Zhang, J. (2020). Experimental Study of Edge-Opened Cracks Propagation in Rock-like Materials. *J. Mining Strata Control. Eng.* 2 (3), 033035. doi:10.13532/j.jmsce.cn10-1638/td.20200313.001

Zhang, J., Ju, Y., and Zhang, Q. (2019). Low Ecological Environment Damage Technology and Method in Coal Mines. *J. Mining Strata Control. Eng.* 1 (1), 013515. doi:10.13532/j.jmsce.cn10-1638/td.2019.02.005

Zhong, D. (2017). Micro-petrology, Pore Throat Characteristics and Genetic Mechanism of Tight Oil Reservoirs – A Case from the 6^{th} and 7^{th} Members of Triassic Yanchang Formation in the Ordos Basin. *Oil Gas Geology.* 38 (1), 49–61. doi:10.11743/ogg20170106

Zhou, N., Lu, S., Wang, M., Huang, W., Xiao, D., Jiao, C., et al. (2021). Limits and Grading Evaluation Criteria of Tight Oil Reservoirs in Typical continental Basins of China. *Pet. Exploration Dev.* 48 (5), 1089–1100. doi:10.1016/S1876-3804(21)60093-9

Zhu, H., Zhong, D., Zhang, T., Liu, G., Yao, J., and He, C. (2018). Diagenetic Controls on the Reservoir Quality of fine-grained "tight" Sandstones: a Case Study Based on NMR Analysis. *Energy Fuels* 32 (2), 1612–1623. doi:10.1021/acs.energyfuels.7b03734

Zuo, J., Yu, M., and Hu, S. (2019). Experimental Investigation on Fracture Mode of Different Thick Rock Strata. *J. Mining Strata Control. Eng.* 1 (1), 013007. doi:10.13532/j.jmsce.cn10-1638/td.2019.02.008

Conflict of Interest: Author JL was employed by the Exploration Department of PetroChina Changqing Oilfield Company.

The authors declare that the research was conducted in the absence of any commercial or financial relationships that could be construed as a potential conflict of interest.